ingegneria sismica
International Journal of Earthquake Engineering
Anno XLIII - Num. 2 - 2026

Optimized design of dynamic characteristics of planetary gear train - based on finite element analysis

Dayu Zhang[1,*]

[1] College of Intelligent Manufacturing of Lishui Vocational and Technical College, Lishui, Zhejiang, 323000, China

SUMMARY: *This research paper formulates dynamic differential equations that take into account the performance of every component within the planetary gear transmission system comprehensively. It also develops calculation methods for stiffness and damping. Finite - element analysis is utilized to compute the particular meshing force among gear components during the system's operation. It also serves to examine the dynamic response traits under the effect of this force. At the same time, we evaluate the effects of different parameter changes on the system's amplitude response to determine the path for optimizing the system's dynamic features.The results of the finite - element analysis show that when an external force is applied to the system, the displacements of the sun gear and other gear elements in the x and y directions fall within the range of -1 to 1 unit. Additionally, the dimensionless meshing force response between the gears can reach up to 1.337 units. The variation of three parameters such as eccentricity error, tooth frequency and shaft frequency error, and damping ratio can lead to a maximum vibration amplitude of 5.625 when the system is stressed, which should be optimized.*

KEYWORDS: *planetary gear train; dynamic modeling; finite element analysis; vibration amplitude*

1 Introduction

Relative to other transmission systems, gear transmission is not only more accurate ratio, higher transmission efficiency, and higher reliability and longer service life [1]. In particular, the planetary gear transmission system also has the advantages of low vibration and noise, large transmission ratio and compact structure, widely used in wind power, aerospace, special equipment and other key industries and projects, its vibration, noise and control issues by the international scientific and technological field of scholars in a wide range of concerns [2-5]. However, as mechanical products and mechanical equipment are increasingly moving towards the direction of high speed, high efficiency, precision, lightweight and automation, the product structure is becoming more and more complex, the speed of product replacement is accelerating, and the performance requirements for the products are getting higher and higher, which requires that the planetary gear transmission system has good dynamic characteristics [6-9]. At the same time, the traditional design method is difficult to comprehensively consider all aspects of the constraints, the obtained is often only a feasible solution to the complex problem, rather than the optimal solution, and it is difficult to meet the requirements of the dynamic characteristics of machinery and equipment, the dynamic characteristics of the system for the optimization of the design can be a large extent to solve such problems [10-13]. It is characterized by solving

*zhangdayu322@163.com
https://doi.org/10.65102/is2026627
Published: 30 April, 2026

the problem in the design stage, and its advantage is that the cost is small and can adapt to the needs of the current fierce market competition.

Regarding the dynamic characteristics of the planetary gear transmission system and its related research, literature [14] established a coupled dynamic model containing time-varying stiffness and friction, analyzed the vibration response under parametric excitation by classifying the lubrication state and numerical solution, and verified the consistency between the simulation and the test, emphasizing the importance of the tooth friction calculation to enhance the accuracy of the model and the optimal design of the planetary gear system. Literature [15] establishes a new dynamic model of planetary gears and analyzes the effects of gear axial tilting and load changes on the dynamic characteristics of the system, pointing out that the tilting reduces the meshing stiffness and significantly changes the higher-order intrinsic frequency and the floating trajectory, and the increase of the load makes the contact from the line to the surface and improves the stiffness, but the lower-order frequency remains stable. For the planetary gear system in aerospace non-inertial system, the literature [16] focuses on analyzing its dynamic characteristics under space motion, and through the establishment of coupled dynamics model, exploring the joint effect of gravity, implicated inertia force, Koch force and gyroscopic moment, pointing out that the non-inertial conditions lead to a significant shift of the radial equilibrium position of the planetary wheel, which reveals the trajectory of each component under different motion conditions, the bearing force and acceleration of the complex rule of change. Literature [17] deduced the equations of motion of each component under arbitrary motion of the fuselage, improved the coupled dynamics model of the non-inertial system, and pointed out that the internal non-inertial system mainly affects the trajectory of the planetary wheel, and the external non-inertial system changes the trajectory of the central component by comparing the dynamic response under different non-inertial conditions, which emphasizes the non-inertial effect significantly affects the bearing force, vibration and load balancing performance, and the traditional method will bring serious errors. For the wind turbine planetary gear system, literature [18] established a nonlinear dynamics model under random wind load, analyzed the effect of stiffness ratio on the dynamic behavior of the system, and found that the variation of the stiffness ratio triggers rich nonlinear dynamics, and the reasonable adjustment can make the system out of the chaos into the stable cyclic motion, while the random load increases the system instability. Literature [19] pointed out that the traditional research is mostly based on the earth reference system, which is inconsistent with the actual working conditions of planetary gears under non-inertial conditions such as aircraft maneuvering, for this reason, it summarizes its commonly used dynamics models and research progress, points out that the dynamics of the non-inertial system is insufficiently researched, and suggests to combine the non-inertial analysis method of the rotor system, and continue to explore the dynamics of the planetary gear system under the non-inertial system in depth.

As a method that can replace complex problems with simpler problems and then solve them, finite element analysis provides support for the optimization of the dynamic characteristics of the planetary gear drive system. FEA views the solution domain as consisting of a number of small interconnected subdomains called finite elements, assumes a suitable approximate solution for each element, and then deduces the total fulfillment conditions for solving this domain to obtain a solution to the problem [20-22]. This method can systematically and effectively evaluate the stress distribution, deformation characteristics and vibration excitation of key components such as gears and shaft systems, so as to reduce the weight or improve the dynamic response through parametric optimization [23, 24]. In the research related to the optimal design of the dynamic characteristics of the planetary gear transmission system, literature [25] for the electric bus planetary gear system, this study through the multi-objective optimization of the gear micro-geometric parameters, and the use of LTCA and modal

superposition method to analyze the dynamic response, the results show that the optimization scheme significantly reduces the vibration and noise of the transmission system, which verifies the validity and safety of the optimization of the design of its dynamic characteristics. Literature [26] pointed out that the traditional method of planetary gear strength calculation with reference to cylindrical gears, the results are conservative and difficult to locate the worst stress point, and through the kinematics and transient finite element analysis, accurately obtain the stress time course of the gears and the location of the maximum stress, which verifies the validity of the method, and lays a foundation for the fatigue analysis and optimal design.

This paper constructs a dynamic model of the planetary gear transmission system, and quantifies the force relationship between the components of the system through equations. Mesh the simplified planetary gear transmission system, establish the contact finite element model of the system gears, iteratively solve the force on each point and surface of the gear transmission contact, and analyze the dynamic response vibration value of the system. Through simulation experiments, to determine the time-varying meshing stiffness for the system's intrinsic frequency, and calculate the vibration displacement data of each component of the system after the force, to analyze the influence of various types of parameters on the amplitude and frequency characteristics of the system vibration, and to determine the direction of optimization of the dynamic characteristics of the system.

2 Finite element-based modeling and analysis of planetary gearing system

2.1 Dynamic model of planetary gearing system

2.1.1 System dynamics modeling

Considering the intricate structure of the planetary gear system, this study constructs its dynamic model using the lumped parameter approach. The stiffness of component supports and the time - varying meshing stiffness of gears are equivalently represented as springs. All components are considered as rigid bodies, incorporating transverse, longitudinal, and torsional degrees of freedom, while multiple error factors are disregarded.Figure 1 depicts the system's dynamic model, with the center of the planet carrier designated as the coordinate origin. Table 1 lists all the parameters of the model and the sub - script definitions for each component.

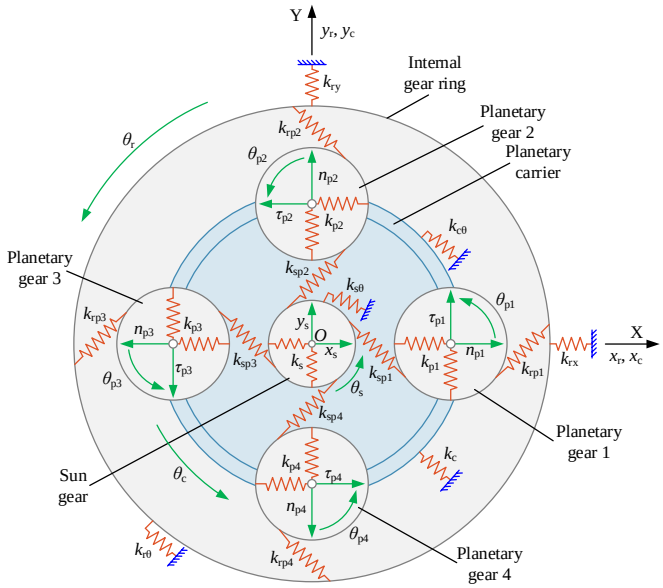

Figure 1: Dynamic Model of Planetary Gear Transmission System

Table 1: Symbols of parameters in the dynamic model

Parameter symbols	Meaning
k_s, k_c, k_r, k_{pi}	Supporting stiffness
$k_{s\theta}$, $k_{c\theta}$, $k_{r\theta}$	Torsional stiffness
k_{spi}, k_{rpi}	Engagement stiffness
x_s, x_c, x_r	Lateral micro-displacement
y_s, y_c, y_r	Longitudinal micro-displacement
n_{pi}	Radial micro-displacement
τ_{pi}	Tangential micro-displacement
θ_s, θ_c, θ_r, θ_{pi}	Torsional angle micro-displacement

The generalized displacement vector of the system can be expressed in the following manner:

$$\{X\}=\{x_s,y_s,\theta_s,n_{pi},\tau_{pi},\theta_{pi},x_c,y_c,\theta_c,x_r,y_r,\theta_r\}^T \tag{1}$$

The tooth profiles of two gears that are meshing with each other stay in close vicinity. There is a linear relationship between the meshing force and the elastic deformation, and a linear spring can be used to simulate the sub - stiffness of the gears. The elastic deformation of the interlocked gear teeth along the meshing line is as follows:

$$\begin{cases}\delta_{spi}=(n_{pi}-x_s)\sin\varphi_{spi}+(y_s-\tau_{pi})\cos\varphi_{spi}+u_s+u_{pi}\\ \delta_{rpi}=(n_{pi}-x_r)\sin\varphi_{rpi}+(y_r-\tau_{pi})\cos\varphi_{rpi}+u_r-u_{pi}\\ \delta_{cpix}=x_c-n_{pi}-u_c\sin\varphi_{pi}\\ \delta_{cpiv}=y_c-\tau_{pi}+u_c\cos\varphi_{pi}\\ \delta_{cpiu}=(n_{pi}-x_c)\sin\varphi_{pi}+(y_c-\tau_{pi})\cos\varphi_{pi}+u_c\end{cases} \tag{2}$$

In this context, the symbols, signify the elastic deformation occurring within the meshing pair between the sun gear, the inner ring, and the third planetary gear. Meanwhile, the symbols,, indicate the projection of the relative displacement between the planetary carrier and the planetary gear along the,, directions. and directions. $\varphi_{spi}(t)=\pi/2+\varphi_{pi}(t)-\alpha_{spi}$; $\varphi_{rpi}(t)=\pi/2+\varphi_{pi}(t)+\alpha_{rpi}$; α_{spi} ; α_{rpi} - pressure angle of the sun wheel, inner gear ring engagement with the i th planetary wheel; $\varphi_{pi}(t)$ - time-varying phase angle of the i th planetary wheel; $\varphi_{pi}(t)=\omega_c t+2\pi(i-1)/4$; ω_c - acceleration of the planetary carrier; $u_s=\theta_s r_s$, $u_r=\theta_r r_r$, $u_{pi}=\theta_{pi} r_{pi}$, $u_c=\theta_c r_c$; r_s, r_r, r_{pi}, r_c - radius of the base circle of the sun wheel, the inner gear ring and the i th planetary wheel and the radius of the planetary carrier.

At this time, the gear pair meshing force is:

$$\begin{cases} F_{spi}=k_{spi}\delta_{spi}+c_{spi}\dot{\delta}_{spi} \\ F_{rpi}=k_{rpi}\delta_{rpi}+c_{rpi}\dot{\delta}_{rpi} \end{cases} \tag{3}$$

Based on the force interaction among the components, the differential equations for the system dynamics are formulated as follows:

$$\begin{cases} m_s\ddot{x}_s+c_s\dot{x}_s-\sum_{i=1}^{4}F_{spi}\cos\varphi_{spi}+k_s x_s=0 \\ m_s\ddot{y}_s+c_s\dot{y}_s+\sum_{i=1}^{4}F_{spi}\sin\varphi_{spi}+k_s y_s=0 \\ \left(I_s/r_s^2\right)\ddot{u}_s+c_{s\theta}\dot{u}_s+\sum_{i=1}^{4}F_{spi}+k_{s\theta}u_s=T_{in}/r_s \\ m_{pi}\ddot{n}_i-k_{pi}\delta_{cpix}\cos\varphi_{pi}-k_{pi}\delta_{cpiv}\sin\varphi_{pi}-F_{spi}\sin\alpha_{spi}+F_{rpi}\sin\alpha_{rpi}=0 \\ m_{pi}\ddot{\tau}_i+k_{pi}\delta_{cpix}\sin\varphi_{pi}-k_{pi}\delta_{cpiv}\cos\varphi_{pi}-F_{spi}\cos\alpha_{spi}-F_{rpi}\cos\alpha_{rpi}=0 \\ \left(I_{pi}/r_{pi}^2\right)\ddot{u}_i-F_{rpi}+F_{spi}=0 \\ m_c\ddot{x}_c+\sum_{i=1}^{4}c_{pi}\dot{\delta}_{cpix}+c_c\dot{x}_c+\sum_{i=1}^{4}k_{pi}\delta_{cpix}+k_c x_c=0 \\ m_c\ddot{y}_c+\sum_{i=1}^{4}c_{pi}\dot{\delta}_{cpiv}+c_c\dot{y}_c+\sum_{i=1}^{4}k_{pi}\delta_{cpiv}+k_c y_c=0 \\ \left(I_c/r_c^2\right)\ddot{u}_c+\sum_{i=1}^{4}c_{pi}\dot{\delta}_{cpiu}+c_{c\theta}\dot{u}_c+\sum_{i=1}^{4}k_{pi}\delta_{cpiu}+k_{c\theta}u_c=T_{out}/r_c \\ m_r\ddot{x}_r+c_r\dot{x}_r-\sum_{i=1}^{4}F_{rpi}\cos\varphi_{rpi}+k_r x_r=0 \\ m_r\ddot{y}_r+c_r\dot{y}_r+\sum_{i=1}^{4}F_{rpi}\sin\varphi_{rpi}+k_r y_r=0 \\ \left(I_r/r_r^2\right)\ddot{u}_r+c_{r\theta}\dot{u}_r+\sum_{i=1}^{4}F_{rpi}+k_{r\theta}u_r=0 \end{cases} \tag{4}$$

Within this formula, the variables represent, in turn, the mass of the sun gear, the nth planetary gear, the planet carrier, and the inner ring. Other damping coefficients correspond to the support

damping and torsional damping of each of the aforementioned components. Additionally, the inertia coefficients signify the rotational transmission inertia of the sun gear, planetary gear, planet carrier, and inner ring respectively.

2.1.2 Calculation of stiffness and damping

In the gear meshing procedure, the stiffness of gear meshing undergoes continuous alterations in tandem with the dynamic deformation of the teeth. It represents the quotient of the normal contact force per unit tooth width to the overall normal deformation of the tooth surface when a pair of standard, error - free spur gears engage at the pitch circle.The ISO strength standard defines two parameters related to meshing stiffness. The initial parameter is the maximum stiffness ratio of the unit tangential meshing force to the normal deformation at the tooth end during the ideal meshing of gears. This ratio provides an approximation of the stiffness at the meshing nodes and critical locations. The second parameter is the stiffness ratio. It is derived by translating the average rotational lag angle of the driven gear into the distance measured along the meshing line during the stable power - transmission process of standard gears.

This research paper utilizes the finite - element approach to compute the time - varying meshing stiffness of gears. For the sun - planet gear and the inner - ring - planet gear, relevant models are constructed to determine the two stiffness values.The inner ring is subjected to fixed constraints to restrict its degrees of freedom, and the radial movement of the sun gear is constrained. When performing the calculations, the torque applied to the sun gear is transformed into nodal forces and exerted on the nodes of its inner ring. The formula for the torque is presented as follows.

$$T = nf_m r_n \tag{5}$$

Here, let: - the total number of nodes on the inner perimeter of the sun gear; - the force exerted by a single node on the inner perimeter of the sun gear; - the radius of the inner perimeter of the sun gear.Then, the force along the direction of the meshing line at this particular point is:

$$F_b = T / r_b \tag{6}$$

where: r_b - The radius of the base circular component of the solar wheel.

When the displacement of the nodes is extracted, if only a single point is extracted, then there will be local singularity on the results, so it is necessary to extract all the node displacements of the inner circle and solve to get its average value, and according to this average value to get the deformation of the inner circle of the sun wheel torsion χ_n. At this time, the rotation angle of the sun wheel along the circumferential direction is:

$$\theta = \chi_n / r_n \tag{7}$$

In order to attain extra rigidity, it is crucial to convert the equivalent rotational angle of the sun gear in the circumferential direction into the direction of the meshing line.

$$\chi_b = \theta r_b \tag{8}$$

At this juncture, the formula for the meshing stiffness between the sun gear and the planet gear can be expressed as:

$$k_{sp} = nf_m r_n^2 / \chi_n r_b^2 \tag{9}$$

Partition a single meshing cycle into segments and construct the relevant finite element model. Implement the computational process described above to determine the meshing stiffness between the sun gear and the planet gear.

Likewise, during the computation of the meshing stiffness between the planetary gear and the inner race, a fixed restraint is imposed on the outer perimeter of the inner race. At the same time, a moment is applied to the inner part of the planetary gear to determine the meshing stiffness of the combination of the planetary gear and the inner race. k_{rp} When calculating the theoretical mesh stiffness, the contact between the gears is set up in accordance with the theoretical mesh pairs in the current mesh position. In the ensuing chapters, when computing the meshing stiffness, to assess the impact of the multi - tooth contact occurrence, aside from establishing the contact between the theoretically contacting meshing pairs, corresponding contacts will also be established for the tooth pairs adjacent to the theoretical contacting pairs. These adjacent pairs might come into contact because of deformation.

In the planetary drive, there are also some parts play a role in transferring power and supporting the function of other transmission components, such as the input shaft supporting the sun wheel. For the stiffness of each supporting member, this paper also chooses the finite element method to solve. The input shaft is taken as an instance to demonstrate the solution approach. The input shaft not only serves to transfer torque but also functions to allow elastic movement for the sun gear.

The input shaft is capable of leveraging flexural deformation to absorb the shock produced when the planetary gear system is in operation. The stiffness of the input shaft, which acts as a measure of its bending deformation, is equal to the support stiffness for the sun gear. When selecting the finite - element method, to prevent local deformation from affecting the results, a central node is defined at the center of the loading end - face, and the nodes on this end - face are coupled with it. The load is applied to the center node, and the deformation of the center node can be obtained by calculation, which is given by $K = F/X$, where X is the deformation of the center node under the action of F , so that the input shaft stiffness can be obtained.

When computing the damping of a system, the system's damping is associated with the mass and stiffness of its adjacent components. Consequently, the mass and rigidity of the gear system can be utilized to compute the equivalent damping of the system.

The formula for equivalent damping is as follows:

$$c_{sp} = 2\xi\sqrt{\frac{k_{sp} m_s m_p}{m_s + m_p}} \tag{10}$$

$$c_{rp} = 2\xi\sqrt{\frac{k_{rp} m_r m_p}{m_r + m_p}} \tag{11}$$

$$c_j = 2\xi\sqrt{k_j m_j}\ (j = s, p, r) \tag{12}$$

The following are the particulars:- The equivalent damping occurring between the sun gear and the planetary gear.- The equivalent damping found between the planetary gear and the internal gear ring.- The damping coefficient.

2.2 Contact analysis of planetary gear trains

2.2.1 Numerical solution for contact finite elements

Contact in finite elements generally refers to the process of two objects coming into contact with each other under the action of a force, and the study of the contact problem in finite elements is mainly concerned with the study of the stress as well as the strain. In dealing with the dynamic contact problem of gears, it is mainly dealt with the help of finite element software.

In the present gear contact problem, the main uncertainty comes from the complexity of the boundary conditions. The intricacy primarily stems from the non - linear nature of the contact breadth of the gear teeth, the clearance on the tooth flanks, the tooth surface irregularities, and the frictional elements. When two independent and related objects are in dynamic contact, the basic equation can be obtained from the finite element contact theory as:

$$\begin{cases} \left[K_A\right]\left\{u_A\right\} = \left\{R_A\right\} + \left\{P_A\right\} \\ \left[K_B\right]\left\{u_B\right\} = \left\{R_B\right\} + \left\{P_B\right\} \end{cases} \tag{13}$$

The stiffness matrix of the two entities is designated as. The nodal displacement matrices of the two entities are signified by and. The overall load matrices of the two entities are presented as and. Moreover, the unit contact force matrices of the two entities are and.

After determining their contact conditions, the stresses and nodal displacements of the two objects in contact can be obtained according to equation (13). Let the contact pairs of the two contacting objects be $i^{(A)}$ and $i^{(B)}\left(i = 1, 2, 3 \cdots n\right)$, respectively, then the contact equations are obtained:

$$\begin{cases} \left\{u_i^{(A)}\right\} = \sum_{i=1}^{N}\left[C_{ij}^{(A)}\right]\left\{R_j^{(A)}\right\} + \sum_{i=1}^{N}\left[C_{ik}^{(A)}\right]\left\{P_k^{(A)}\right\} \\ \left\{u_i^{(B)}\right\} = \sum_{i=1}^{N}\left[C_{ij}^{(B)}\right]\left\{R_j^{(B)}\right\} + \sum_{i=1}^{N}\left[C_{ik}^{(B)}\right]\left\{P_k^{(B)}\right\} \end{cases} \tag{14}$$

where i, j, k for the node number, $\{R_j^{(A)}\}$, $\{R_j^{(B)}\}$ for the contact points i, j, respectively, the vector of internal forces; $\{P_k^{(A)}\}$, $\{P_k^{(B)}\}$ for the role of the node k on the vector of external forces; $C_{ik}^{(A)}$, $C_{ik}^{(B)}$ for the node k unit of force acting on the deformation caused by the i points.

The equation of the contact pair is:

$$\left\{u_i^{(B)}\right\} = \left\{u_i^{(A)}\right\} + \left\{\delta_0\right\} \tag{15}$$

If Eq. satisfies Equation $\left\{R_j^{(B)}\right\} = \left\{R_j^{(A)}\right\} + \left\{R_j\right\}$, substituting this equation into Eq. (14) yields Eq:

$$\sum_{i=1}^{N}\left[c_{ij}\right]\left\{R_j\right\} = \left\{\delta^k\right\} + \left\{\delta^0\right\} \tag{16}$$

where δ^k is the external force loading displacement vector. If a torque is applied to the object,

it is obtained in the contact equation:

$$\sum_{i=1}^{N} R_{ji} r_i = T_p \tag{17}$$

By solving the above equations together, the overall contact matrix equation can be derived when two objects are in contact with each other. See equation (17) The contact equation is solved iteratively until the results converge. During the solution process, the extreme values of the contact pairs of the internal force vectors are deleted, and then a new flexible matrix is created before solving again. The unit contact matrix equation is obtained as follows.

$$\begin{bmatrix} C_{11} & C_{12} & \cdots & C_{1j} & \cdots & C_{12} & r_1^{(A)} & r_1^{(B)} \\ \vdots & \vdots & \cdots & \vdots & \cdots & \vdots & \vdots & \vdots \\ C_{i1} & C_{i2} & \cdots & C_{ij} & \cdots & C_{i2} & r_i^{(A)} & r_i^{(B)} \\ \vdots & \vdots & \cdots & \vdots & \cdots & \vdots & \vdots & \vdots \\ C_{n1} & C_{n2} & \cdots & C_{ni} & \cdots & C_{nm} & r_n^{(A)} & r_n^{(B)} \\ r_1^{(A)} & r_2^{(A)} & \cdots & r_j^{(A)} & \cdots & r_n^{(A)} & 0 & 0 \\ r_1^{(B)} & r_2^{(B)} & \cdots & r_j^{(B)} & \cdots & r_n^{(B)} & 0 & 0 \end{bmatrix} \begin{bmatrix} R_1 \\ \vdots \\ R_i \\ \vdots \\ R_n \\ \theta_1 \\ \theta_2 \end{bmatrix} = \begin{bmatrix} \delta_1^{(2)} \\ \vdots \\ \delta_i^{(2)} \\ \vdots \\ \delta_n^{(2)} \\ T_P^{(1)} \\ T_P^{(1)} \end{bmatrix} \tag{18}$$

2.2.2 Contact finite element modeling of gears

1) Contact type setting

Within the contact categorization of the finite element software Abaqus, there exist two contact methods: one is founded on surface contact, and the other is centered around contact units. Which Abaqus/Standard mode can be used based on the face contact and contact unit based contact, usually gears of the static mechanics of the contact analysis is to use the mode, while Abaqus/Explicit mode can only be used based on the face of the contact, the general gears of the display of the dynamics of the analysis of the use of this mode of analysis.

There exist two primary types of face - based interaction: one is the individual - to - individual interaction mode, and the other is the surface - to - surface interaction mode.

There exist two types of contact methods: point - to - point contact and face - to - face contact.In point - to - point contact, the nodes on the slave surface establish contact with their corresponding projected nodes on the master surface. The fundamental principle of this contact mode is that the slave nodes are less densely distributed compared to the master nodes. Furthermore, the slave nodes are not allowed to pierce through the master surface. In contrast, the master nodes have the ability to penetrate the slave surface. Face - to - face contact is another frequently used discrete contact method. The principles for its selection are as follows: the smaller surface is designated as the slave surface. When the stiffness is the same, the mesh with larger elements is regarded as the master surface. Also, the contact surface with a larger contact area is preferably set as the master surface.

2) Load Setting and Degree of Freedom Constraints

The structure of the planetary gear transmission system is intricate. Therefore, this research primarily examines the contact condition among the sun gear, planet gears, and the internal gear ring. The planet carrier is regarded as a rigid body and is not involved in the contact analysis; instead, it is substituted with kinematic constraints. Since each planet gear has the same contact relationship, just one gear is chosen for analysis to decrease the computational burden. Subsequently, the simplified model is meshed using Hypermesh.

In the course of the contact analysis, the scale of mesh discretization has an impact on the

precision of the outcomes. The mesh within the gear contact area is refined, while the mesh at the gear body and the rim is made less fine.

The planetary gear transmission system, which was segmented in Hypermesh, is transferred to Abaqus. In Abaqus, a contact finite - element model is built for the internal gear ring, the sun gear, and the planet gear. To define the contact relationship, the surface - to - surface contact method is employed within Abaqus. This face - to - face contact is detected and evaluated via the Gaussian points on the surface. The contact region on the contact surface consists of a sequence of Gaussian points. In the definition of the master and slave surfaces should be satisfied: choose the surface with relatively large stiffness as the master surface, and because there are two pairs of contact pairs in the contact model, it is best to choose only one as the master surface in the contact surface. In this research paper, the epicyclic gear engages with both the central gear and the inner gear ring. Consequently, the contact area of the epicyclic gear is always chosen as the main surface.

The flow of finite element simulation is depicted in Figure 2. The following are the procedures for setting up contact analysis in Abaqus.

a) Within the material properties, allocate an elastic modulus of 210 gigapascals and establish Poisson's ratio at 0.45.

b) Allocate material characteristics to the components of the driveline. Then, set up the coupling point (that is, the MPC unit) at the center of the circular shape of each gear. Subsequently, incorporate the hinge connection relation to delineate the transmission relation between the sun gear and the planetary gear.

c) First, set up the direct interaction among the internal gear ring, the central gear, and the planetary gear. After that, define the contact characteristics. Given that the time - varying meshing stiffness of the gears has been calculated in the field of dynamics, the average value is chosen to ascertain the contact stiffness.

d) Begin the analysis phase. At the start of this analysis phase, initially impose restrictions on the axial movement of the sun gear, the planetary gear, and the internal gear ring.

e)To begin with, the inner gear ring is subjected to fixed boundary limitations, while reasonable freedom constraints are established for the sun gear and planet gears. A minuscule rotation angle is applied to the sun gear. This action serves to eliminate the gaps within the gear pairs, enabling close contact between the gears. Moreover, it guarantees that the iterative calculation will converge during the subsequent contact analysis.

f) The second phase of the analysis entails applying the angle of rotation to the sun gear. After that, load and torque are exerted on the coordinate system defined by the hinge. The hinge connection is used to simulate the interaction between the planet gear and the planet carrier in the planetary drive mechanism.

g) Compute the contact stresses, bending stresses, and the submission procedures of the gear pair for an analytical solution.

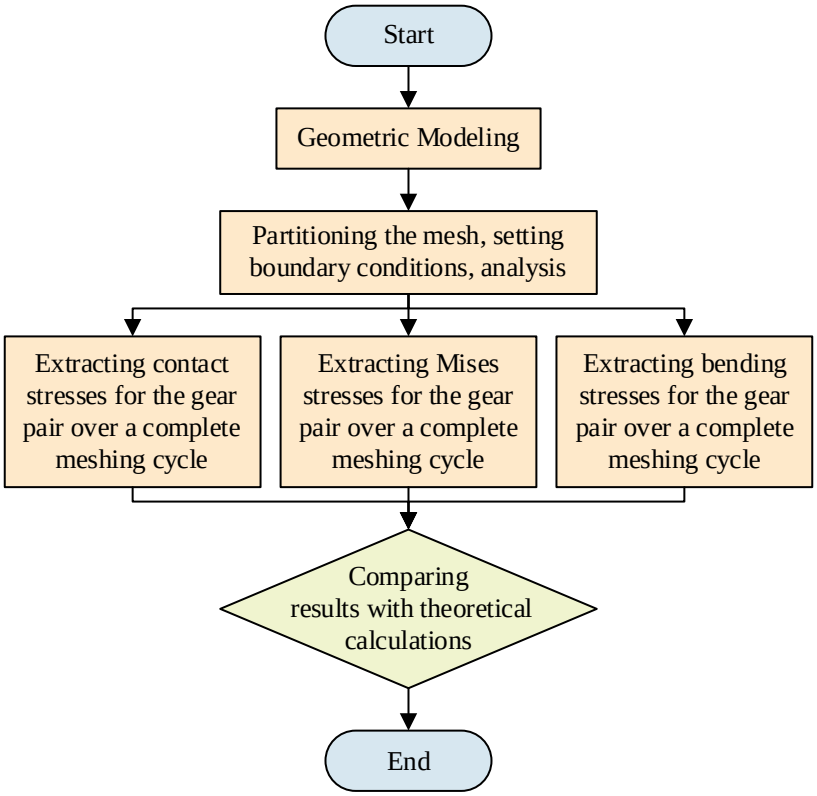

Figure 2: Finite element simulation flow chart

2.3 Dynamic response analysis of planetary gear system

2.3.1 Planetary gear system characteristics

During the meshing procedure of gear transmission systems, a variety of excitations will unavoidably trigger system vibration and noise. This kind of vibration directly impacts the system's rigidity, structural robustness, and operational lifespan. By integrating the system's intrinsic traits and input excitation circumstances, the system's vibration response can be determined.Figure 3 presents the transfer characteristics of the system. Given the time - varying internal dynamic excitation, the transient dynamic approach is employed to determine the system response. In this section, Abaqus software is utilized to conduct a finite element simulation of the dynamic response of the planetary gear system.

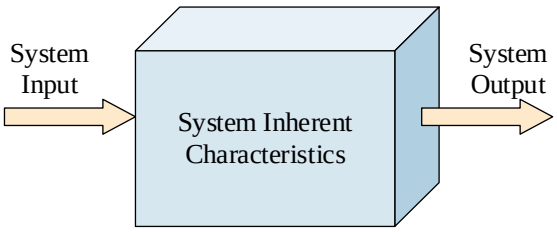

Figure 3: System Transfer Characteristics

2.3.2 Theory of system response analysis

By solving the system's dynamic equations, considering the known input excitation and its inherent characteristics, the amplitude of the system's vibrational response can be determined.The equation that governs the motion in Abaqus transient dynamics is presented as

follows:

$$[M]\{\ddot{x}\}+[C]\{\dot{x}\}+[K]\{x\}=\{F(t)\} \tag{19}$$

Among them:

- A matrix that depicts the system's mass; - A matrix that portrays the system's damping; - A matrix that illustrates the system's stiffness; - A matrix that exhibits the system's displacement; - A matrix that displays the system's velocity; - A matrix that represents the system's acceleration.

At a specific discrete point in time, the above equations can be viewed as hydrostatic equations that simply take into account inertial and damping forces, and it is by solving for consecutive discrete points that Abaqus obtains the values of the system's vibrational response over the entire time period.

In Abaqus, there are three techniques for analyzing transient dynamics, namely the full method, the simplified method, and the modal superposition approach.

Complete Method: The complete matrix is used, which makes the calculation more accurate; it is simple to use as it does not require the selection of principal degrees of freedom; it allows any type of load to be added; and, crucially, it allows the presence of nonlinearities in the model, which makes it highly applicable. However, because the complete method uses a complete matrix and involves nonlinearities, it has higher requirements for computer hardware.

Modal superposition approach: the system's response value is acquired by multiplying the eigen - values by a specific factor and then adding them together. This stands in contrast to the complete approach, where the outcomes are achieved through direct computation. This method allows the addition of damping, and for the nonlinear case, only point-to-point contact is considered; and the time step must be guaranteed to be constant throughout the analysis, but the method is not very demanding on the hardware.

Reduction method: the size of the problem is compressed by reducing the matrix dimension and choosing the principal degrees of freedom, and then the results on the principal degrees of freedom are extended to the complete set of degrees of freedom to obtain a complete solution of the system. The method initially computes only the solution on the main degrees of freedom, thus the loads must all be added in the direction of the main degrees of freedom; it is faster compared to the complete method.

The modal superposition method is suitable for solving forced vibration problems of elastic systems with multiple degrees of freedom. The basic idea is that the original coupled n equations are decoupled by coordinate transformation, and the mass and stiffness matrices are converted to diagonal matrices. Ultimately, the solution of the equations of motion can be represented as a linear combination of a sequence of solutions for the vibration equations with a single degree of freedom. Moreover, the solution for each individual degree of freedom can be simplified to the issue of Duhamel integral. Subsequently, the solution is converted into the response values in the original coordinates through the application of coordinate transformations.

The equations with a single degree of freedom are usually solved by means of the Duhamel integral. This approach involves decomposing the excitation force into a large number of minuscule shocks. Subsequently, the responses associated with each of these minute shocks are aggregated to compute the total response of the system.

According to the result of the Duhamel integral, the response of the r - d order mode can be expressed in the following manner:

$$\begin{cases} q_i(t) = \dfrac{1}{\omega_i^2}\int_0^t f_i(\tau)e^{-\xi_i\bar{\omega}_i(t-\tau)}\sin\bar{\omega}_i\left(t-\tau\right)d\tau + e^{-\xi_i\bar{\omega}_i t}\left(A_i\sin\bar{\omega}_i t + B_i\cos\bar{\omega}_i t\right) \\ f_i(\tau) = \phi^T\left\{F(\tau)\right\}\phi \end{cases} \tag{20}$$

ϕ-vector of modal shapes

$f_i(\tau)$-Magnitude of the component of excitation on each vibration mode

$\bar{\omega}_i, \omega_i$-Value of the i th order intrinsic frequency of the damped and undamped system

A_i, B_i-Constant calculated from the initial conditions

$\bar{\omega}_i \to \omega_i$ when the damping ξ_i is so small that it tends to 0, i.e. $\xi_i \to 0$, at which point the i th order modal response $q_i(t)$ becomes:

$$q_i(t) = \frac{1}{\omega_i}\int_0^t r_i(\tau)\sin\omega_i\left(t-\tau\right)d\tau + a_i\sin\omega_i t + b_i\cos\omega_i t \tag{21}$$

Subsequently, in accordance with [the reference], the values of each level of vibration mode are combined to determine the value of the system's vibration response at the instant of [the specific time].

$$x(t) = \sum_{i=1}^{n}\phi_i q_i(t) \tag{22}$$

3 Dynamic characteristic analysis and optimization practice of planetary gearing system

3.1 Driveline Dynamics Analysis

3.1.1 Inherent characteristics of the system

The system possesses inherent dynamic traits in the form of natural frequency and vibration. When the frequency of external excitation gets close to the system's natural frequency, resonance takes place. By examining these intrinsic attributes, one can direct the dynamic optimization design of planetary gear transmission systems.

This research paper employs a four - stage planetary gear mechanism as an example. The main parameters of this computational instance are shown in Table 2. The 4 major categories of this system have a total of 11 subcategories of intrinsic characteristic-related parameters, all of which are increasing with the increase of the level. For example, the mass of the first stage sunwheel is 0.241kg, the mass of the second sunwheel increases to 0.643kg, the mass of the third sunwheel increases to 1.753kg, and the mass of the fourth wheel reaches 2.078kg.

Table 2: The main parameters of the example

Inherent characteristics		Level 1	Level 2	Level 3	Level 4
Mass	Sun gear mass (kg)	0.241	0.643	1.753	2.078
	Planetary gear mass (kg)	0.575	0.851	3.815	4.917
	Planetary carrier mass (kg)	1.893	2.462	14.721	20.496
Base circle radius	Base circle radius of the sun gear (mm)	13.652	20.173	31.758	37.845
	Base circle radius of the planetary gear (mm)	40.254	41.654	45.276	50.716
	Equivalent radius of the planetary carrier (mm)	60.492	64.537	79.625	85.911
Moment of inertia	Moment of inertia of the sun gear ($kg \cdot mm^2$)	19.375	354.162	2537.376	57743.751
	Moment of inertia of the planetary gear ($kg \cdot mm^2$)	571.163	665.256	5748.275	94865.198
	Moment of inertia of the planetary carrier ($kg \cdot mm^2$)	6082.317	86354.195	136547.627	197653.804
Engagement stiffness	External engagement equivalent engagement stiffness (N/mm)	$9.271x10^6$	$10.867x10^6$	$11.346x10^7$	$15.764x10^7$
	Internal engagement equivalent engagement stiffness (N/mm)	$1.642x10^7$	$2.754x10^7$	$4.751x10^8$	$6.347x10^8$

Figure 4 depicts the system modes of the algorithm under equivalent meshing stiffness. Here, the horizontal axis represents the degrees of freedom of the system components, while the vertical axis corresponds to their intrinsic vibration modes. Additionally, f(i) denotes the i - th order natural frequency. Fig. 4(a) shows the degrees of freedom and the corresponding intrinsic vibration modes of the first to fourth order planetary frames. Fig. 4(b) shows the degrees of freedom and the corresponding intrinsic vibration patterns of one to four levels of sun wheels. Fig. 4(c) shows the degrees of freedom and the corresponding intrinsic vibration patterns of one to four levels of planetary wheels.

The motion of the system is examined within a plane that has translational and rotational degrees of freedom, which encompass displacement and rotational patterns. As depicted in Figure 4, the natural frequencies of this system span from 204.483 Hz to 1321.636 Hz, and there is no zero - frequency rigid - body mode. When delving into the system's intrinsic properties, adjusting the system's natural frequency can cause it to diverge from the external interference frequency. This prevents the onset of resonance and improves the accuracy of the dynamic characteristics' optimal design.

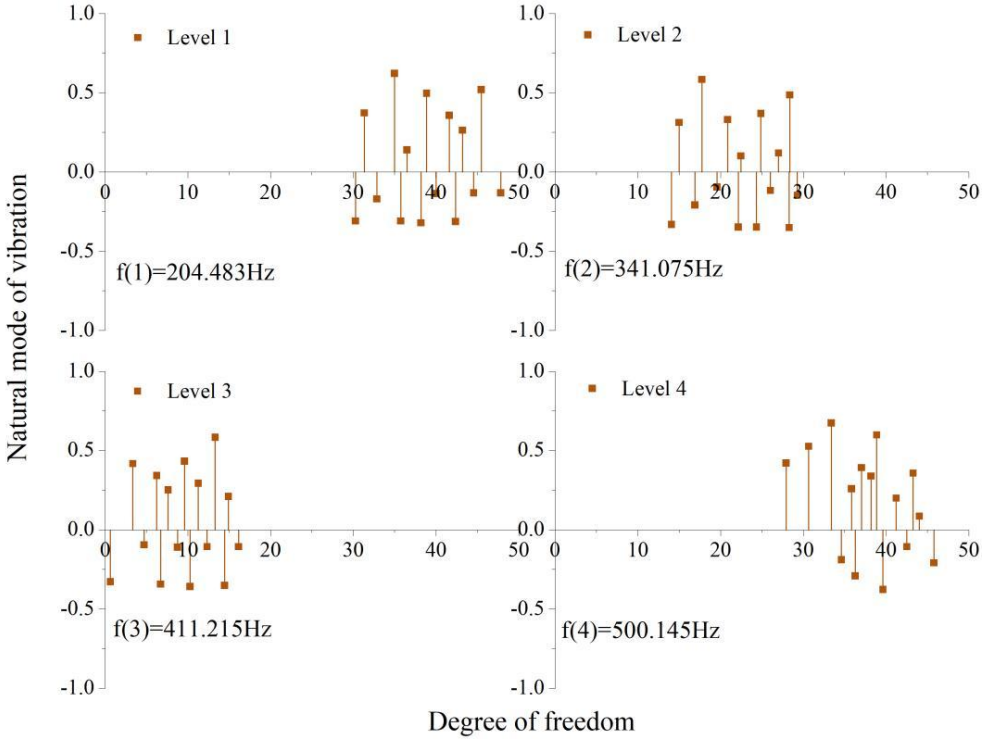

(a) The system modes of planetary gear levels 1 to 4

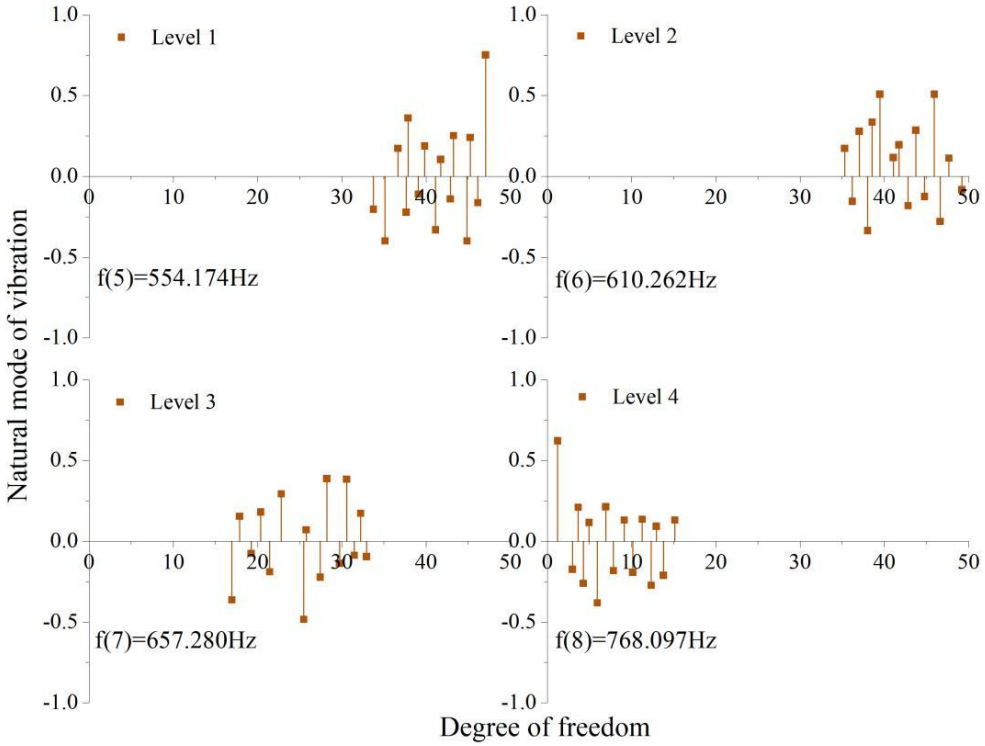

(b) The system modes of the Sun Wheel levels 1 to 4

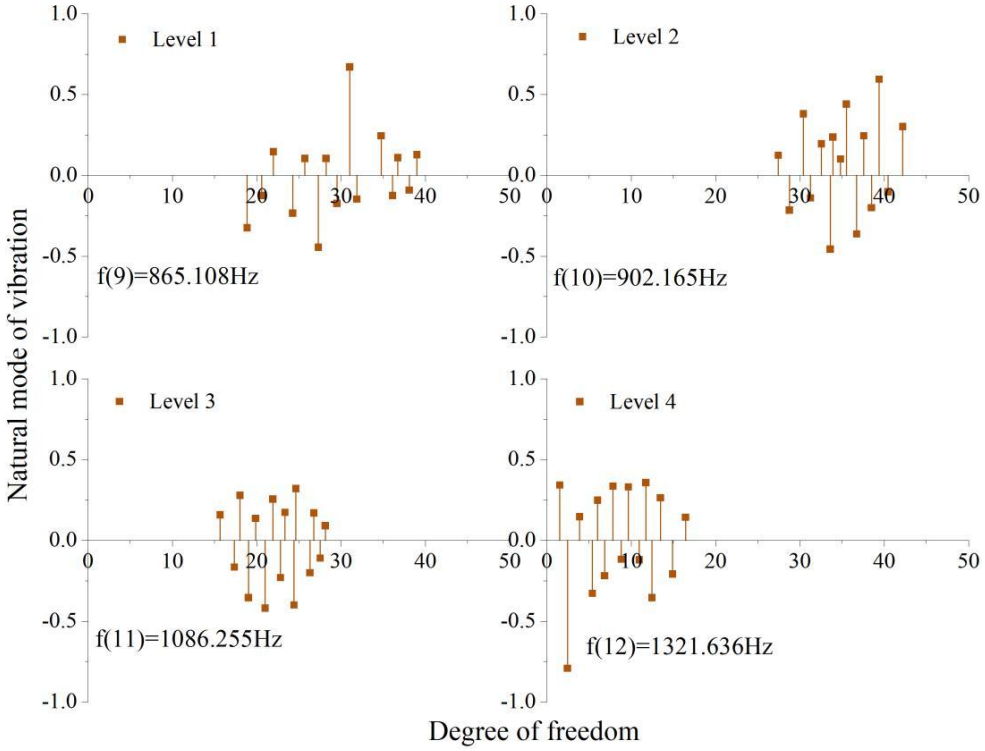

(c) The system modalities of planetary gears 1 to 4 levels

Figure 4: System modal under equivalent meshing stiffness

3.1.2 Time-varying meshing stiffness solution

The natural frequency of the system is influenced by the time - varying meshing stiffness. The variation pattern of this stiffness is presented in Figure 5. The meshing stiffness oscillates between 7.087 N/mm and 13.481 N/mm, and correspondingly, the natural frequency undergoes synchronous alterations.

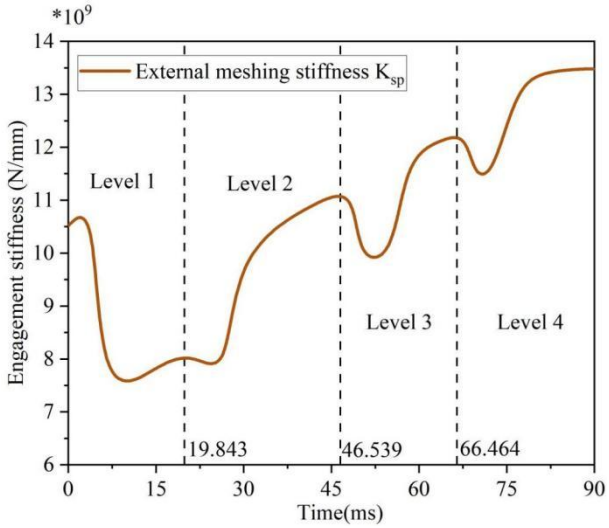

Figure 5: The variation of time-varying meshing stiffness over time

3.2 Dynamic Response Characterization

3.2.1 Analysis of vibration displacement response of system components

The system dynamic differential equations are resolved using the finite element approach. During the computation, the transient and unstable outcomes from the initial phase are excluded, and only the subsequent steady - state solutions are kept. To analyze the central motion path of each component, the translational vibration displacement curves of every gear part and the torsional meshing force curves of meshing pairs are obtained.

Figure 6 illustrates the translational vibration displacement response curves for the sun gear, two - stage planet carriers, and planet gears. The excitation period is represented on the horizontal axis. The vibration displacement intervals for each component along the x - axis and y - axis directions are presented independently. This indicates that there are notable disparities in the vibration amplitudes of all the components.

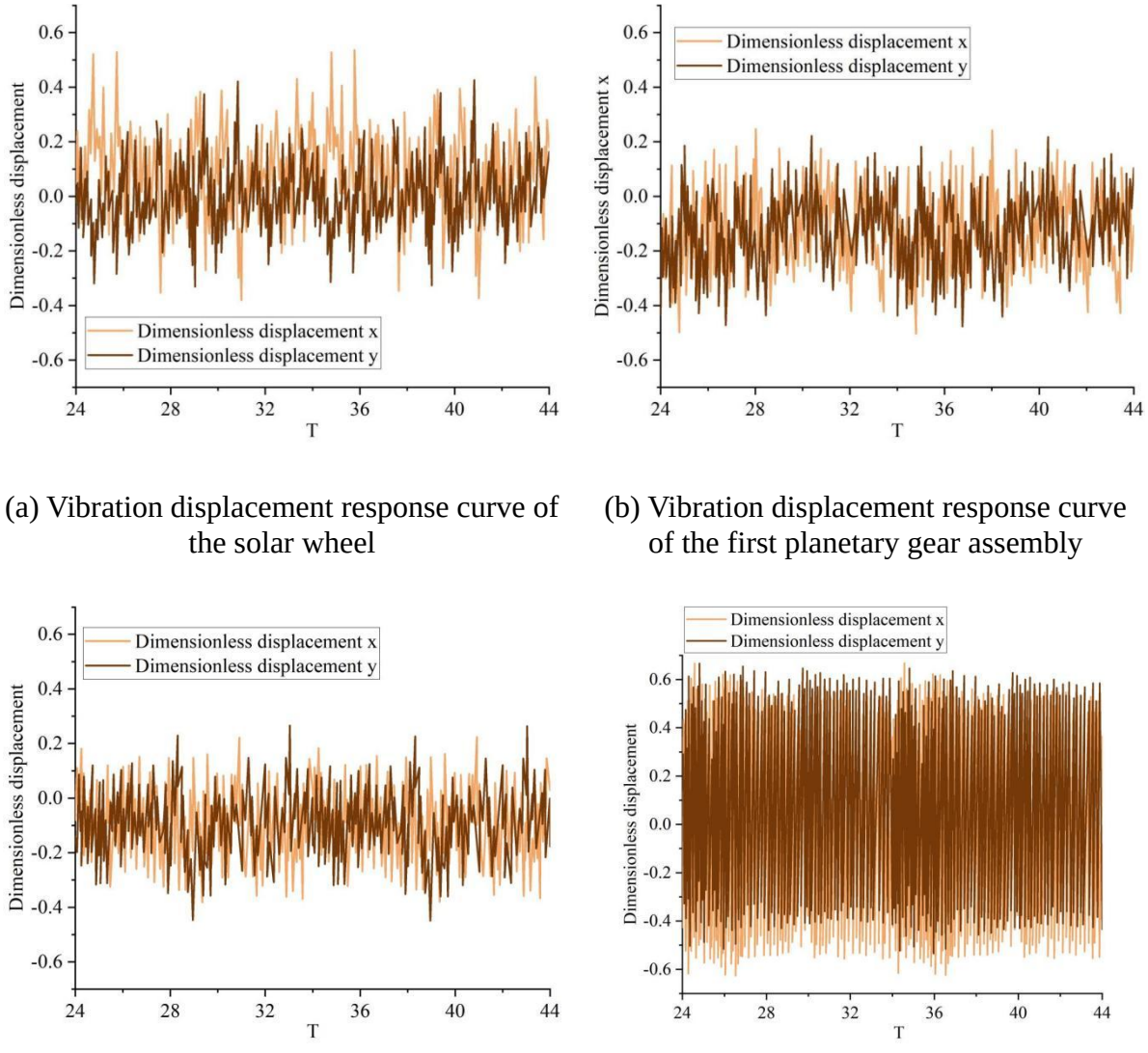

(a) Vibration displacement response curve of the solar wheel

(b) Vibration displacement response curve of the first planetary gear assembly

(c) Vibration displacement response curve of the second planetary gear assembly

(d) Vibration displacement response curve of the planetary gear

Figure 6: Vibration displacement response of component in translational direction

3.2.2 Analysis of the meshing force response of the meshing pair between the sun wheel and each planetary wheel

The meshing force response curves of each gear pair are presented in Figure 7. The dimensionless meshing force of each gear pair fluctuates within specific, separate ranges.

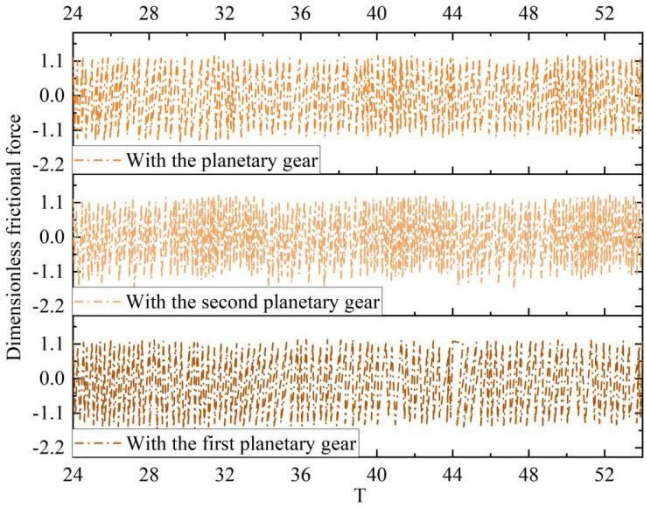

Figure 7: Response curve of the meshing force of the meshing pair Sn

3.2.3 Trajectory of the center of the system components

The motion trajectories of the component centers within the gear system are presented in Figure 8. The central motion paths of the sun gear, planet gear, first planet carrier, and second planet carrier are intricate and non - regular. However, their range of variation is limited, falling between -1 and 1. This indicates that when torque T is exerted on the system, it triggers a dynamic reaction in each component, resulting in displacement. The movement of each component can be computed via finite element analysis.

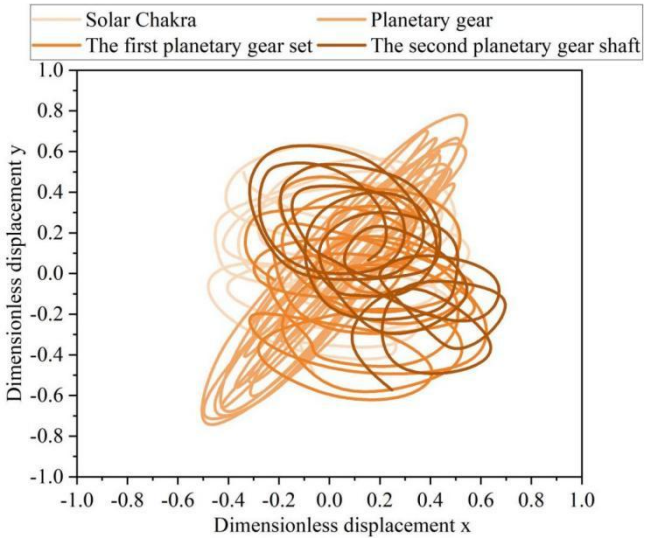

Figure 8: Motion trajectories of the centers of each component in the gear system

3.3 System amplitude-frequency characteristic analysis

3.3.1 Analysis of the effect of eccentricity error on the amplitude-frequency characteristics of the system

As the torque increases, the rotational speed of the system goes up, which in turn modifies the dynamic characteristics and vibration amplitude of the gear pair. This research paper examines the impacts of parameters on the amplitude - frequency characteristics through finite element analysis, taking into account only the gear eccentricity error. When specific simulation parameters are set, the system's vibration undergoes significant alterations under the influence of the eccentricity error. The mean vibration value reaches its peak around $\Omega = 2.5$, and the vibration amplitude hits its maximum at $\Omega = 2.63$. Moreover, the vibration amplitude increases more rapidly as the rotational speed climbs.

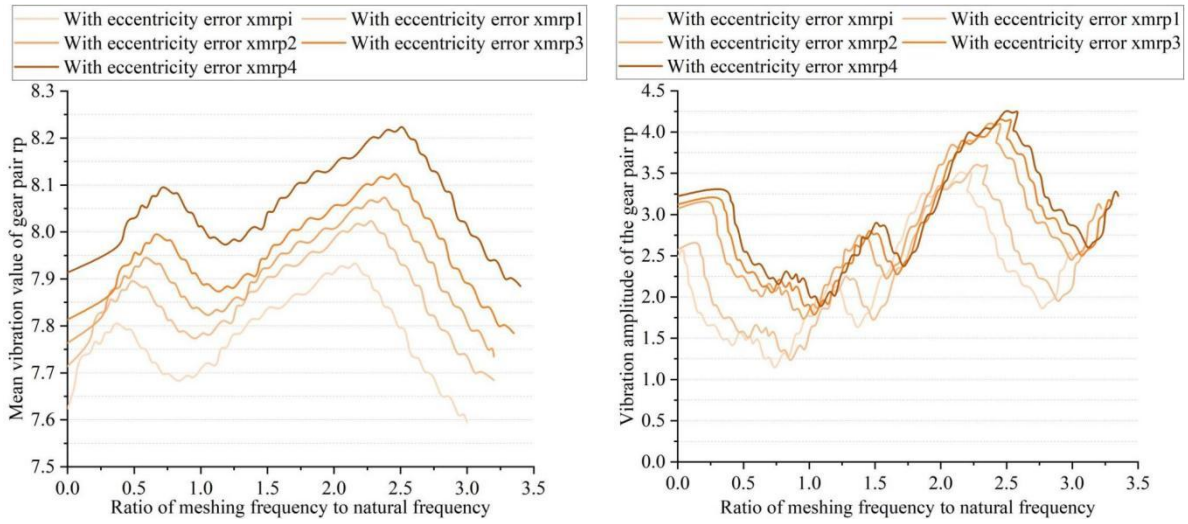

(a) Mean vibration value of gear pair rp (b) Vibration amplitude of the gear pair rp

Figure 9: The influence of eccentricity error on system vibration amplitude

3.3.2 Analysis of the effect of tooth frequency and shaft frequency errors on the amplitude-frequency characteristics of the system

In this research paper, only the system tooth frequency and shaft frequency errors are considered, with the simulation parameters remaining constant. For the simulation, specific pre - determined error values are established, and only the outcomes of the rp gear pair are examined. Figure 10 presents the root - mean - square (RMS) value and the amplitude of the system's vibration. These errors will significantly increase the system's average vibration level and vibration amplitude. Additionally, as the rotational speed goes up, the rate of increase becomes even more pronounced. When Ω is approximately 2.5, the vibration amplitude of each rp gear pair reaches its peak, with the maximum amplitude being 3.966.Due to the differences in eccentricity phases, the response amplitudes of each gear pair vary. The error of eccentricity exerts an influence on the load - sharing performance of the system.

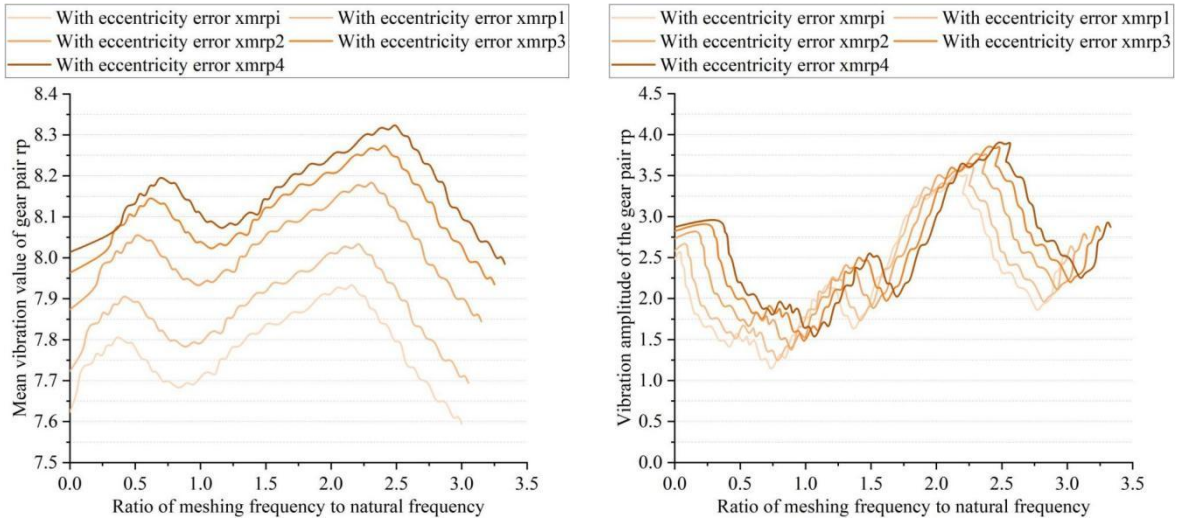

(a) Mean vibration value of gear pair rp (b) Vibration amplitude of the gear pair rp

Figure 10: System vibration amplitude under tooth and axial frequency error

3.3.3 Analysis of the effect of damping ratio on the amplitude-frequency characteristics of the system

Excluding other error components, only the tooth frequency and shaft frequency errors of the system are taken into account. When the ratio of the meshing frequency to the intrinsic frequency, denoted as Ω, ranges from 0 to 3.5, with a torque (Tp) of 300 N - m and a damping ratio (ζ) of 0.15, and only the results of the rp gear pair are presented, Figure 11 depicts the mean vibration and vibration amplitude of the system. The damping ratio has a notable impact on the system's vibration amplitude, causing it to vary significantly. When ζ=0.15, the system amplitude is small, only 0.339~1.697, and the global amplitude curve is continuous. When ζ=0.09, the system vibration amplitude reaches the maximum of 3.570~5.625, and the instability interval increases, gradually changing from stable engagement to unilateral shock, bilateral shock and other states.

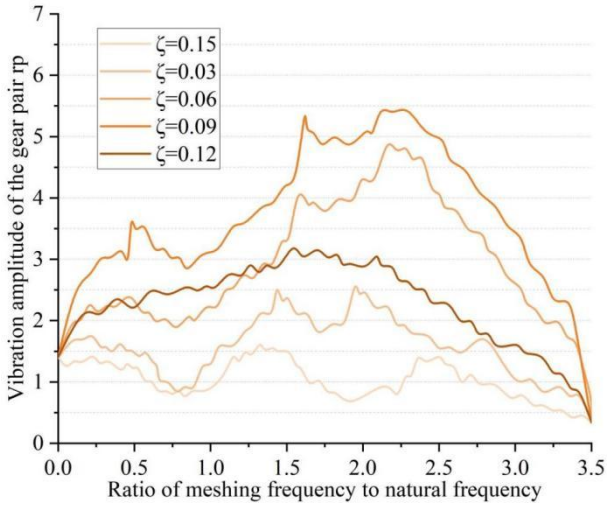

Figure 11: Overall influence of damping ratio on amplitude of system vibration

4 Conclusion

This research paper constructs a dynamic model for the planetary gear transmission system. It then utilizes finite - element analysis to investigate the vibration response traits during its operation. In the meshing frequency ratio span from 0 to 3.5, several elements such as gear eccentric error, frequency deviation of teeth and shafts, and the damping factor all have a significant negative impact on the system's vibration amplitude. Specifically, when Ω equals 2.5, the vibration amplitude in the presence of tooth frequency and shaft frequency error is 3.966. Moreover, when the damping ratio (ζ) is 0.09, the system's vibration amplitude can reach 5.625.To enhance the stability of the planetary gearing system, it is crucial to make every possible effort to minimize the eccentricity error, the tooth frequency and shaft frequency error, and the damping ratio of the system. Additionally, the system's ability to withstand external impacts should be improved.

About the Author

Dayu Zhang came into the world in Datong, Shanxi Province, People's Republic of China, in 1986. He earned a master's degree from Nanjing Tech University. At present, he is employed at the College of Intelligent Manufacturing of Lishui Vocational and Technical College. His primary area of research is mechanical design and production.

References

[1] Habermehl, C., Jacobs, G., & Neumann, S. (2020). A modeling method for gear transmission efficiency in transient operating conditions. Mechanism and Machine Theory, 153, 103996.

[2] Wang, C. (2019). High power density design for planetary gear transmission system. Proceedings of the Institution of Mechanical Engineers, Part C: Journal of Mechanical Engineering Science, 233(16), 5647-5658.

[3] Xu, X., Fan, X., Diao, P., & Liu, H. (2019). An investigation on the influence of modification parameters on transmission characteristics of planetary gear system. Journal of Mechanical Science and Technology, 33(7), 3105-3114.

[4] Fan, Z., Zhu, C., & Song, C. (2020). Dynamic analysis of planetary gear transmission system considering the flexibility of internal ring gear. Iranian Journal of Science and Technology, Transactions of Mechanical Engineering, 44(3), 695-706.

[5] Zhang, C., Wei, J., Niu, R., Hou, S., & Zhang, S. (2023). Similarity and experimental prediction on load sharing performance of planetary gear transmission system. Mechanism and Machine Theory, 180, 105163.

[6] Yuan, J., Lyu, B., Hang, W., & Deng, Q. (2017). Review on the progress of ultra-precision machining technologies. Frontiers of mechanical engineering, 12(2), 158-180.

[7] Wei, B. (2025). INTEGRATED PATH AND EFFICIENCY ANALYSIS OF AUTOMATION CONTROL AND MECHANICAL DESIGN. Global Media and Social Sciences Research Journal, 6(02), 490-496.

[8] Ruibo, C., Jianxing, Z., & Wenlei, S. (2018). Dynamic characteristics of a planetary gear system based on contact status of the tooth surface. Journal of mechanical science and technology, 32(1), 69-80.

[9] Xiang, L., Gao, N., & Hu, A. (2018). Dynamic analysis of a planetary gear system with multiple nonlinear parameters. Journal of Computational and Applied mathematics, 327, 325-340.

[10] Che, X., & Zhu, R. (2023). Dynamic behavior analysis of planetary gear transmission system with bolt constraint of the flexible ring gear. Meccanica, 58(7), 1173-1204.

[11] Yang, L., Yuan, B., Gong, J., Qin, M., & Liu, G. (2023). Dynamic modelling and vibration characteristics of a marine compound gear transmission system. Proceedings of the Institution of Mechanical Engineers, Part K: Journal of Multi-body Dynamics, 237(2), 261-278.

[12] Wang, J., Chen, X., Bi, X., Mo, R., & Yi, Y. (2025). Research on Nonlinear Dynamic Characteristics of TBM Gear Transmission System with Novel Double Compound Planetary Gears. Journal of Vibration Engineering & Technologies, 13(7), 511.

[13] Li, W., Sun, J., & Yu, J. (2019). Analysis of dynamic characteristics of a multi-stage gear transmission system. Journal of Vibration and Control, 25(10), 1653-1662.

[14] Xiao, Z., Chen, F., & Zhang, K. (2021). Analysis of dynamic characteristics of the multistage planetary gear transmission system with friction force. Shock and Vibration, 2021(1), 8812640.

[15] Chen, R., Zhou, J., & Sun, W. (2018). Dynamic characteristics of a planetary gear system based on contact status of the tooth surface. Journal of Mechanical Science and Technology, 32(1), 69-80.

[16] Wei, J., Shi, L., Zhang, A., & Qin, D. (2019, August). Modeling and dynamic characteristics of planetary gear transmission in non-inertial system of aerospace environment. In International Design Engineering Technical Conferences and Computers and Information in Engineering Conference (Vol. 59308, p. V010T11A019). American Society of Mechanical Engineers.

[17] Wei, J., Zhang, A., Shi, L., Qin, D., & Lim, T. C. (2020). Modeling and dynamic characteristics of planetary gear transmission in non-inertial system of aerospace environment. Journal of Mechanical Design, 142(3), 031103.

[18] Yang, H., Li, X., Xu, J., Yang, Z., & Chen, R. (2021). Dynamic characteristics analysis of planetary gear system with internal and external excitation under turbulent wind load. Science Progress, 104(3), 00368504211035604.

[19] Gao, B., Wang, Y., & Yu, G. (2023). Research Progress on the Dynamic Characteristics of Planetary Gear Transmission in a Non-Inertial System. Machines, 11(7), 751.

[20] Welch-Phillips, A., Gibbons, D., Ahern, D. P., & Butler, J. S. (2020). What is finite element analysis?. Clinical spine surgery, 33(8), 323-324.

[21] Thompson, M. K., & Thompson, J. M. (2017). ANSYS mechanical APDL for finite element analysis. Butterworth-Heinemann.

[22] Erhunmwun, I. D., & Ikponmwosa, U. B. (2017). Review on finite element method. Journal of Applied Sciences and Environmental Management, 21(5), 999-1002.

[23] Xiao, Z., Cao, J., & Yu, Y. (2020). Mathematical Modeling and Dynamic Analysis of Planetary Gears System with Time-Varying Parameters. Mathematical Problems in Engineering, 2020(1), 3185624.

[24] Wang, S., & Cao, Y. (2022). Analysis of planetary gear transmission characteristics based on ANSYS. Journal of Engineering Research and Reports, 23(1), 22-32.

[25] Zhang, Q., Xu, S., Yuan, Y., Yan, X., Huang, D., Yu, J., ... & Nguyen, T. T. (2023). Multi-objective optimization design and dynamic characteristic analysis based on planetary gear transmission. Journal of Network Intelligence, 8(3), 639-657.

[26] Zeng, Q., Jiang, S., Wan, L., & Li, X. (2015). Finite element modeling and analysis of planetary gear transmission based on transient meshing properties. International Journal of Modeling, Simulation, and Scientific Computing, 6(03), 1550035.